Macromolecular Materials and Engineering
www.mame-journal.de

New Insights into Segmental Packing, Chain Dynamics and Thermomechanical Performance of Aliphatic Polyurea Composites: Comparison between Silica Oxides and Titanium (III) Oxides

*Khanisya Palaniandy, Sheik Ambarine Banon Auckloo, Giuseppe Cavallaro, Eng Seng Chan, and Pooria Pasbakhsh**

Polyurea (PU) is intrinsically reinforced by its microphase-separated morphology, giving its excellent mechanical properties. In this study, it is shown how a high-index PU formulation applies easy diffusion of hard segments into the soft phase of the PU matrix and tune its chain mobility. Moreover, the interaction of micro (>100 nm), nano (<100 nm) fillers with the microdomains and their thermomechanical properties are unraveled. Herein, nanosilica oxide (NS) and micro titanium (III) oxide (Ti_2O_3) are incorporated at low loadings into a solvent-free two-component aliphatic PU via *insitu* polymerization. While NS achieves an interfacial interaction with urea groups and forms a tight hard segmental packing, the large-sized Ti_2O_3 assembles the interconnected PU chain network, improving its crystallinity. Strong reinforcement by NS is noticed when tensile strength increased from 26 to 31 MPa and on the maximum thermal degradation temperature by 21 °C increment from the neat PU. In contrast, the soft segmental dynamics are triggered with the presence of Ti_2O_3 as indicated in the reduction in glass transition temperature and the 288% improvement in the storage modulus. This study provides an insightful perspective in designing robust PU composites, effective for myriad applications including strong and flexible films in circuit boards and photovoltaic (PV) cells.

1. Introduction

Polyurea (PU) is an elastomer exhibiting a wide range of physical, mechanical, and chemical properties such as abrasion resistance, leather appearance, viscoelasticity, water insensitivity, etc.[1] It is derived from a step-growth polymerization of a diisocyanate (–NCO) with amines ($–NH_2$) to form urea linkages, cross-linked with extensive hydrogen (H) bonds .[2] Bidentate H-bonding formed between these urea linkages acts as a physical crosslinker between two PU chains. PU also has a self-assembled phase-separated microstructure consisting of both hard segments (HS) and soft segments (SS) as a result of their thermodynamic incompatibility.[3] HS and SS are both responsible for their enhanced modulus, high resiliency to withstand deformation, and high extensibility.[4] This unique elastomer has found interesting applications in military armor coatings,[5–7] concrete coatings,[8–10] bridge reinforcement,[11,12] and explosion-proof vehicles.[13]

PU is classified into two types based on the structure of the diisocyanates used; aromatic and aliphatic. It was reported that aliphatic PU demonstrates more excellent light stability, higher resistance to hydrolysis, higher resistance to thermal degradation, and lower reactivity as compared to aromatic ones.[14] Li et al.[15] reported that the phase separation of aliphatic HSs-based PU is significantly complete owing to the higher chain mobility. Corcuera et al.[16] also supported that aliphatic PU exhibit higher HS crystallinity and superior thermal stability, however, due to different morphology formed, aromatic PU exhibited higher ductility, higher tensile strength, and lower modulus.[17] Even the aliphatic diisocyanates exhibit varying mechanical properties due to their segmental packing and planarity. The bulky isophorene diisocyanate (IPDI) is regarded as loosely packed hard domains with freely moving chain segments whereas the linear and symmetric hexamethylene diisocyanate usually assembles into tight packing with restricted chain mobility.[18] Better hard domain packing strongly increases the extent of

K. Palaniandy, S. A. B. Auckloo, P. Pasbakhsh
Mechanical Engineering Discipline, School of Engineering
Monash University Malaysia
Jalan Lagoon Selatan, Bandar Sunway, Subang Jaya 47500, Malaysia
E-mail: pooria.pasbakhsh@monash.edu
G. Cavallaro
Department of Physics and Chemistry
University of Palermo
Viale delle Scienze, pad. 17, Palermo 90128, Italy
E. S. Chan
Chemical Engineering Discipline, School of Engineering
Monash University Malaysia
Jalan Lagoon Selatan, Bandar Sunway, Subang Jaya 47500, Malaysia

The ORCID identification number(s) for the author(s) of this article can be found under https://doi.org/10.1002/mame.202100582

DOI: 10.1002/mame.202100582

microphase separation leading to improvement in modulus, hardness, and tear strength.[19,20]

The HS is usually made of diisocyanates and low molecular weight amine chain extenders. Chain extenders are used to lengthen the HS size during the polymerization and they force the urea functionalities close to each other, which increases the formation of H-bonds.[2,21] Cai et al. synthesized aliphatic PU without the use of chain extenders and obtained tensile strength of only 2.2 MPa. Conversely, Qian et al.[22] synthesized aliphatic PU using similar components with the addition of an aromatic chain extender reported higher tensile strength of 13.1 MPa, owing to the more excellent proximity of urea groups. Additionally, the types and ratios of different chain extenders influence the processing conditions and mechanical properties of PU. Iqbal et al.[2] reported that aromatic chain extenders are more reactive than their aliphatic counterparts, which led to shorter gel-time and a higher ratio of aromatic to aliphatic chain extender resulted in higher storage modulus and lower dissipation potential. Therefore, an optimal ratio of aromatic to aliphatic chain extender could tune the reactivity and properties of PU to the desired results.

In the presence of moisture, isocyanates are hydrolyzed and broken down into unstable carbamide and form amine groups, which could react with more isocyanates to form urea moieties. Typically, a 105% rule is used for the NCO/NH_2 ratio in PU formulation, whereby the five percent excess isocyanates accounts for loss upon reacting with residual moisture during storage and transportation. Past studies[23,24] have reported that the excess NCO in PU enables a higher degree of crosslinking resulting in higher yield stress and lower failure strain. However, the increase in mechanical properties reaches a plateau and decreases when there is over excess of NCO due to the rise in internal stress in the matrix. It was noticed that such a situation arises in fast curing formulations, whereby the gel time is achieved as soon as the reactants are mixed homogenously, entrapping the internal stress within the matrix. So far, the use of over-excess NCO (index > 2.0) has not been exploited for achieving high yield stress in slower curing formulations.

Synthesis of PU involves the addition of toxic and volatile organic solvents to facilitate the reaction (mainly to reduce the high viscosity of amine mixture), which creates significant human and environmental health concerns. In response to these hazards, several solvent-free routes to PU exist in the new literature.[25–27] Synthesis of poly(dimethylsiloxane) based-semicrystalline PU with tunable crystalline melting points exhibited high strain at break between 495% and 1180%, as reported by Sirrine et al.[25] However, the low HS content (4.0 wt%) led to an ultimate tensile strength of only 1.16 MPa. On the other hand, a non-solvent route using diphenyl carbonates[27] achieved higher stress and elongation at break results of 17 MPa and 681%, respectively. However, multi-step polymerization was used incurring in longer processing time, which is not suitable for an industrial-scale application. Thus, there is a strong need for producing solvent-free PU with excellent properties using simpler approaches.

Although PU is intrinsically reinforced by its morphology, recent studies[22,28–30] showed that the inclusion of reinforcing fillers is a promising way to enhance its mechanical and thermal stability and induce hydrophobicity effects. This is important so that it opens an avenue for PU to be employed in newer applications including heat dissipating coatings in printed circuit boards,[31] shock absorbers in fuel cells,[32] and antireflective coatings in PV cells.[33] A wide variety of fillers have been integrated into PU matrix in the past like carbon nanotubes,[34–36] carbon black,[37,38] nanoclays,[39,40] glass fibers,[13,41] and graphenes.[42–44] However, the studies on metal oxide or metalloid oxides including zinc oxide, titanium-based oxides (TiO, TiO_2, or Ti_2O_3), or silica oxides-based PU composites, to our best knowledge, are limited. Casalini et al.[39] reported that nanoclays (layered silicates) did not improve the tensile strength and toughness of aromatic PU effectively due to the increase in viscosity in the prepolymer solution giving defects in the final product (entrapped air, inhomogeneous dispersion, etc.). The fact that 1D silicates requiring exfoliation or intercalation to achieve homogenous dispersion itself are an added complexity. 3D nanosized silica oxides on the other hand, have shown promising results[29,45–47] owing to their higher surface area but it has not been explored in aliphatic-based PU, to the best of our knowledge. It is also worth noting that the nano-reinforcement effect is observed significantly in PU with a higher crosslinking degree as it enhances stress transfer across the composite matrix.

The properties of composites are profoundly connected to the dispersion of the fillers; thus, significant efforts have been put into achieving homogenous dispersion in the base matrix. One of these is the in situ polymerization technique where either the polymer is synthesized in the solution containing fillers or filler particles are synthesized in the polymer solution.[48,49] This method gives a more controlled and well-defined polymer-filler network with many of the studies have relied on solvents for better dispersion.[34,43,50] Very few studies directly integrated the fillers into the PU solution; thus, this study aims to achieve strong interaction between the fillers and PU with this method under the sonication condition.

Inspired by these motivations, we synthesized solvent-free aliphatic PU with a high NCO to NH_2 ratio (index) using a one-step polymerization reaction and allowed it to cure at ambient conditions. The films were further reinforced by adding silica oxide nanofiller and titanium (III) oxide microfiller, respectively, via *insitu* polymerization. The prepared aliphatic PU and its composites were characterized to compare their chemical, mechanical, thermal, physical, and morphological properties.

2. Experimental Section

2.1. Materials

IPDI was purchased from Sigma Aldrich. Polyoxypropylene diamines (Jeffamine D2000 and aliphatic chain extender, Jeffamine D230 equivalent) with molecular weights of 2000 and 230 g mol^{-1}, respectively were purchased from Qingdao Iro Chemical Ltd. Aromatic chain extender, diethyltoluenediamine (Ethacure E100 equivalent), was purchased from Qingdao Iro Chemical. Ltd as well. Hydrophilic-fumed silica oxide nanoparticles (Aerosil 200) with a surface area of 200 $m^2\ g^{-1}$ were purchased from Evonik. Titanium (III) oxide, Ti_2O_3 micro-sized powder of ≈325 mesh size (1–2 μm) was purchased from Alfa Aesar. The properties of all the raw materials and reinforcing materials used in this experiment are listed in Tables S1 and S2, Supporting

Table 1. Composition by mass of PU and PU composites.

Reinforcing material	Designation	IPDI [g]	D2000 [g]	D230 [g]	E100 [g]	Reinforcing material [g]
-	PU	10	19.5	0.6	0.6	-
Silica oxide	PU/0.5% NS	10	19.5	0.6	0.6	0.154
	PU/1% NS	10	19.5	0.6	0.6	0.307
Titanium (III) Oxide	PU/0.5% Ti_2O_3	10	19.5	0.6	0.6	0.154
	PU/1% Ti_2O_3	10	19.5	0.6	0.6	0.307

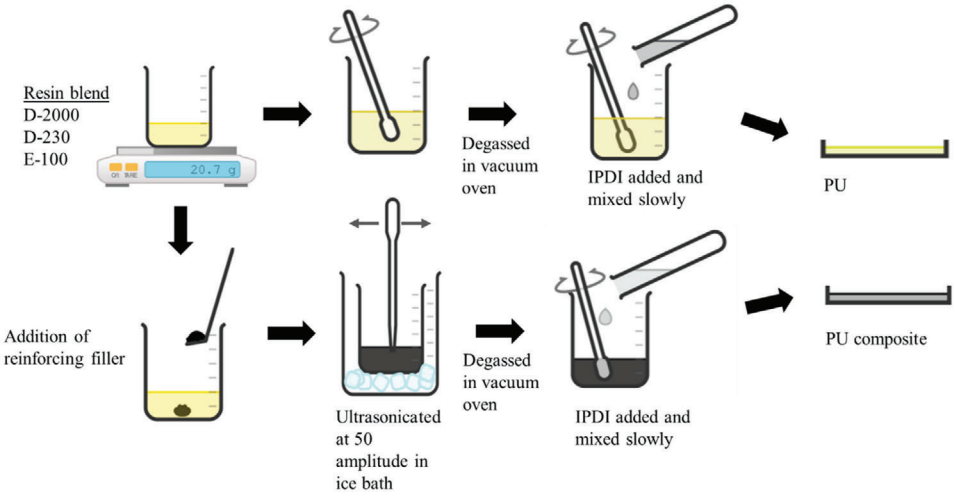

Figure 1. Preparation method of solvent-free PU and PU composites.

Information, respectively. All the materials were dried in a vacuum oven to remove air cavitation and entrapped moisture.

2.2. Synthesis of Aliphatic PU Composites

Table 1 lists the composition of all samples by mass. The index and HS content of the aliphatic PU formulation used in this study were calculated using Equations S1 and S2, Supporting Information. The PU in this study yields an index of 2.77 (2.77 higher NCO equivalent group than NH_2 equivalent groups) with 36.48% HS content. To prepare the B-side solution, D2000, D230, and E100 were mixed in a beaker as shown in **Figure 1**. The mixture in the beaker was then degassed in a vacuum oven (no temperature applied) until there was no more air cavitation. The desired amount of reinforcing material corresponding to the percentage weight used was added into the mixture. The mixture was stirred until a homogenous solution was obtained. The solution was sonicated in the ice bath at 50 amplitude for 20 min. The temperature of this mixture was heated to around 80 to 95 °C and maintained to reduce its viscosity before mixing with IPDI. The temperature of the B-side should not exceed 120 °C as it reaches the flashpoint of D230. The viscosity reduction will ensure vacuum void-free PU films. After heating, the B-side solution was mixed with IPDI and stirred slowly until a homogenous solution was obtained. The temperature and viscosity values of the B-side before and after mixing with IPDI are listed in Table S3, Supporting Information. The mixture was degassed to ensure zero air cavitation before casting on a petri dish. The mold was kept at room temperature in a desiccator for 13 days to remove any moisture in the film. Then, the films were post cured at 80 °C for 24 h. The same procedure was followed to prepare neat PU without the addition of filler and sonication steps. The samples were labeled as PU for neat sample, PU/NS for silica oxide, and PU/Ti_2O_3 for titanium (III) oxide with their corresponding filler content.

2.3. Characterization of PU Composites

Fourier-transform infrared (FTIR) spectroscopy technique was employed to determine the chemical bonding present in the samples. After post-curing in the oven, the sample was taken out and cooled down to room temperature for 30 min. The FTIR program was set to collect 64 scans for absorbance versus wavenumber.

A uniaxial tensile test was carried out using Instron 5966 Universal tensile machine with a crosshead speed of 500 mm min^{-1}. The samples were cut into dumbbell shape following ISO 37 type 2 standard with a test length of 20 mm using a hydraulic press. Three specimens were tested and the average tensile strength and average elongation at break values were recorded.

Hardness test was performed using a digital handheld Shore D durometer of range 0–100HD and five readings were taken and averaged. The values were determined within a few seconds once the reading was stabilized.

Dunnet ordinary one-way ANOVA statistical analysis was performed for the tensile and hardness test data in reference to the neat PU with a 95% confidence interval. In the discussion, data

with p-value < 0.05 is referred to as significant data, and p-value > 0.05 is described as non-significant data.

Perkin Elmer differential scanning calorimetry (DSC) was used to determine the glass transition temperature by heating the specimens (5–10 mg) from −50 to 50 °C with a heating rate of 10 °C min^{-1}.

The thermal degradation of PU and PU composites was tested using thermogravimetric (TGA) analysis. The temperature range of all samples was set to room temperature to 600 °C with a heating rate of 10 °C min^{-1}. Modulated TGA data have been collected by using a TGA 550 (Discovery series – TA Instrument) apparatus. Each sample (≈10 mg) was heated up with a modulated temperature ramp consisting of an average heating rate of 2 °C min^{-1} and an oscillation amplitude of 5 °C with an oscillating period of 200 s. A nitrogen flow was used during heating. MTGA results have been analyzed using real-time deconvolution techniques (discrete Fourier transformation) to obtain the activation energy values (E_a) as functions of the extent of conversion without assumption on the degradation model.[51]

The viscoelastic properties of PU and PU-based nanocomposites were investigated through Dynamic mechanical analysis (DMA). DMA experiments were carried out using a DMA Q800 apparatus (TA Instruments) in the oscillatory regime (frequency of 1.0 Hz). The strain amplitude was set at 0.5%, while the temperature was varied from 30 to 180 °C with a rate of 4 °C min^{-1}. The measurements were performed using a shear sandwich clamp.

The surface characteristics of the samples were examined under the field emission scanning electron microscope (FE-SEM) with an acceleration voltage of 3 to 15 kV and an X-ray diffractometer (XRD) with a wavelength of 0.154 nm. Bragg's law was used to determine the distance between the lattice plane of atoms, d-spacing.

$$d = \frac{\lambda}{2\sin(\theta)}, where\ \lambda = 0.154\ nm \quad (1)$$

The surface wettability of the samples was tested via the water contact angle technique. A macro magnifying lens was placed on a smartphone with a high-resolution camera feature on a stand perpendicular to the sample. The sample was placed on a glass slide fixed to a retort stand. A warm light bulb was placed behind the glass slide perpendicular to the sample, and a whiteboard was placed in front of the bulb to avoid the light from overpowering the shots. A 0.1059 mm needle was fixed to a syringe to produce a micro-sized water droplet on the sample surface. 10 images were collected at an interval of 30 s and they were analyzed using the Low Bond Asymmetric Drop Shape method.[52] The change in water contact angle with time was fitted by an empiric approach based on the following equation.[53]

$$\theta(t) = \theta_i e^{-k_\theta t^n} \quad (2)$$

where θ_i corresponds to the initial water contact angle, k_θ and n are characteristic coefficients related to the overall contact angle and physicochemical phenomena involved in the kinetic process. n specifically range from 0 and 1 relying on the water absorption and spreading contributions to the kinetic θ evolution.

3. Results and Discussion

3.1. Aliphatic PU and PU Composites

Figure 2 shows the contact transparency of the PU and PU composites films. The calorimetric results for PU, PU/0.5%NS, and PU/1% Ti_2O_3 are presented in Table S4, Supporting Information, to show the overall color and chroma change on PU with the addition of fillers. Lightness, L^* is measured as 0 for ideal black colors and 100 for ideal white colors.[54] According to the calorimetric test, PU/0.5%NS is slightly lighter and PU/1%Ti_2O_3 is much darker than neat PU due to the color differences of the two fillers (white for NS and violet-black for Ti_2O_3). However, the appearance of the film did not change significantly with the addition of silica oxide as confirmed by the color change, ΔE values for PU/1% Ti_2O_3 is much greater (26.55) with respect to the reference sample, neat PU as compared to PU/0.5% NS (1.66). The neat sample demonstrated the best contact transparency, brightest and clearest among all the samples, with the highest chroma, C^* value among the rest (PU/0.5%NS) and PU/1%Ti_2O_3). As a general fact, fillers of size smaller than wavelength of light minimizes the light scattering phenomena, thus reducing the loss of transparency and reduces the overall color change.[55] Therefore, from the calorimetric and contact transparency results, silica oxide nanofiller had the lowest effect on the appearance of PU film.

3.2. Fourier Transform Infrared Radiation (FTIR)

The chemical interaction and the occurrence of characteristic bonds of PU are detected using the Fourier transform infrared radiation (FTIR) analysis. The characteristic bonds of each raw material are indicated in Figure S1, Supporting Information. The disappearance of the N═C═O peak at 2259 cm^{-1} from the isocyanate monomer, IPDI, for the neat PU in **Figure 3**a indicates the complete conversion of the NCO[56] on the 13th day. Since there are excess NCO groups, hydrolysis of NCOs in the presence of moisture from air form unstable carbamic acid compounds, which eventually break down into more NH_2 available to react with remaining NCOs to form urea linkages and carbon dioxide, CO_2.[57] Therefore, the mixture was properly degassed to allow the release of CO_2 out of the samples. The reaction between the NCO and NH_2 groups had led to the formation of characteristic bands of HS and SS in PU. The peaks at 3327 to 3486 cm^{-1}[58,59] in Figure 3b are associated with NH stretching bonds which constitute NH-free bonds at 3486 cm^{-1} and bonded NH at 3327 cm^{-1}. Similarly, the occurrence of hydrogen-bonded carbonyl (C═O) bonds is detected at 1630 cm^{-1}[60] in Figure 3d. The bending of NH and stretching of CO simultaneously in the urea linkage, NH–C═O molecule is observed at 1557 cm^{-1}.[58] The C–H stretching bands (Figure 3c) and the C–O aliphatic ether bond (Figure 3e) at 1096 cm^{-1} are retained from the SS contributed by diisocyanate and polyamine chains.

In general, three types of C═O and N–H bonds are described in PU; "free" without hydrogen bonding, "disordered" or monodentate where hydrogen bond forms between single NH and single CO, and "ordered" where hydrogen bond forms between single CO molecule with two NH molecules known as bidentate hydrogen bonding.[61] Bidentate hydrogen bonding forms a more regular structure than monodentate hydrogen bonding. The absence

Figure 2. Contact transparency of PU and PU composites samples prepared in this study.

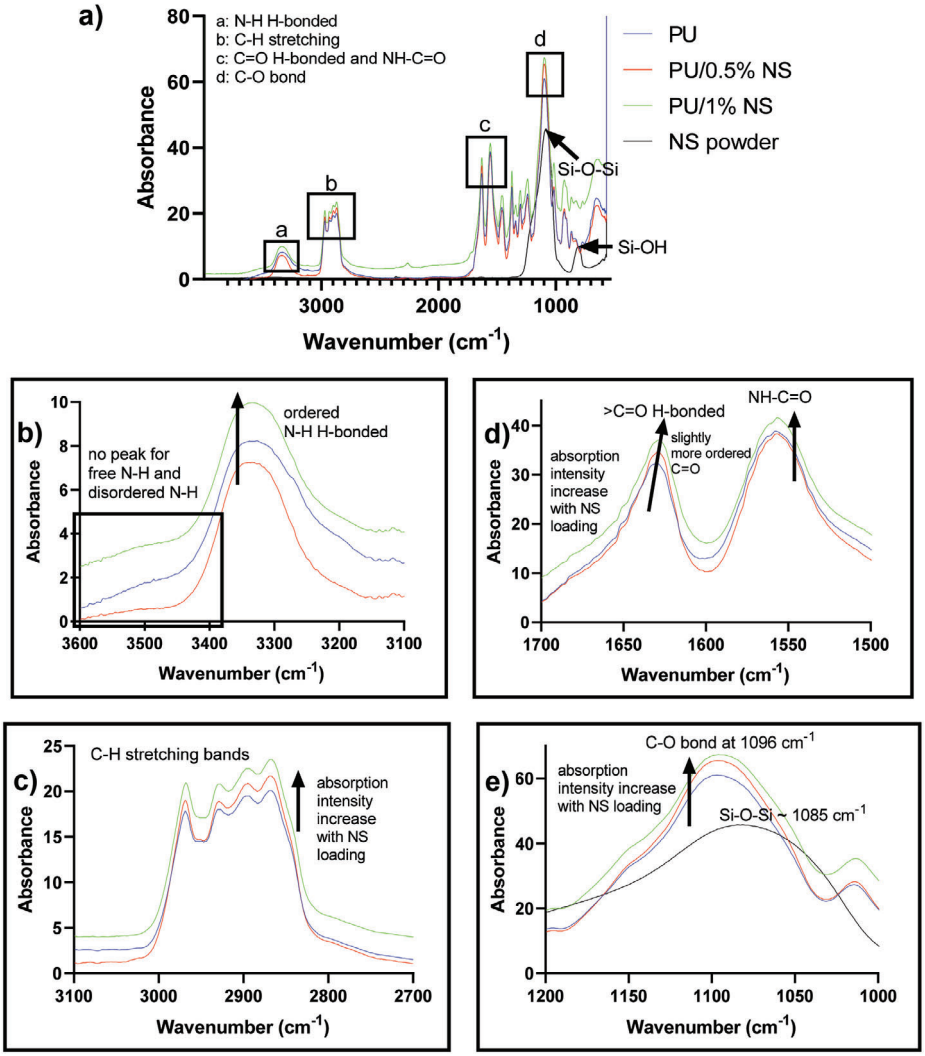

Figure 3. Superimposed FTIR spectra of PU with different loadings of silica oxide, NS, a) full spectra, b) N–H H-bonded region, c) C–H stretching region, d) carbonyl H-bonded region, e) ether, C–O bond region.

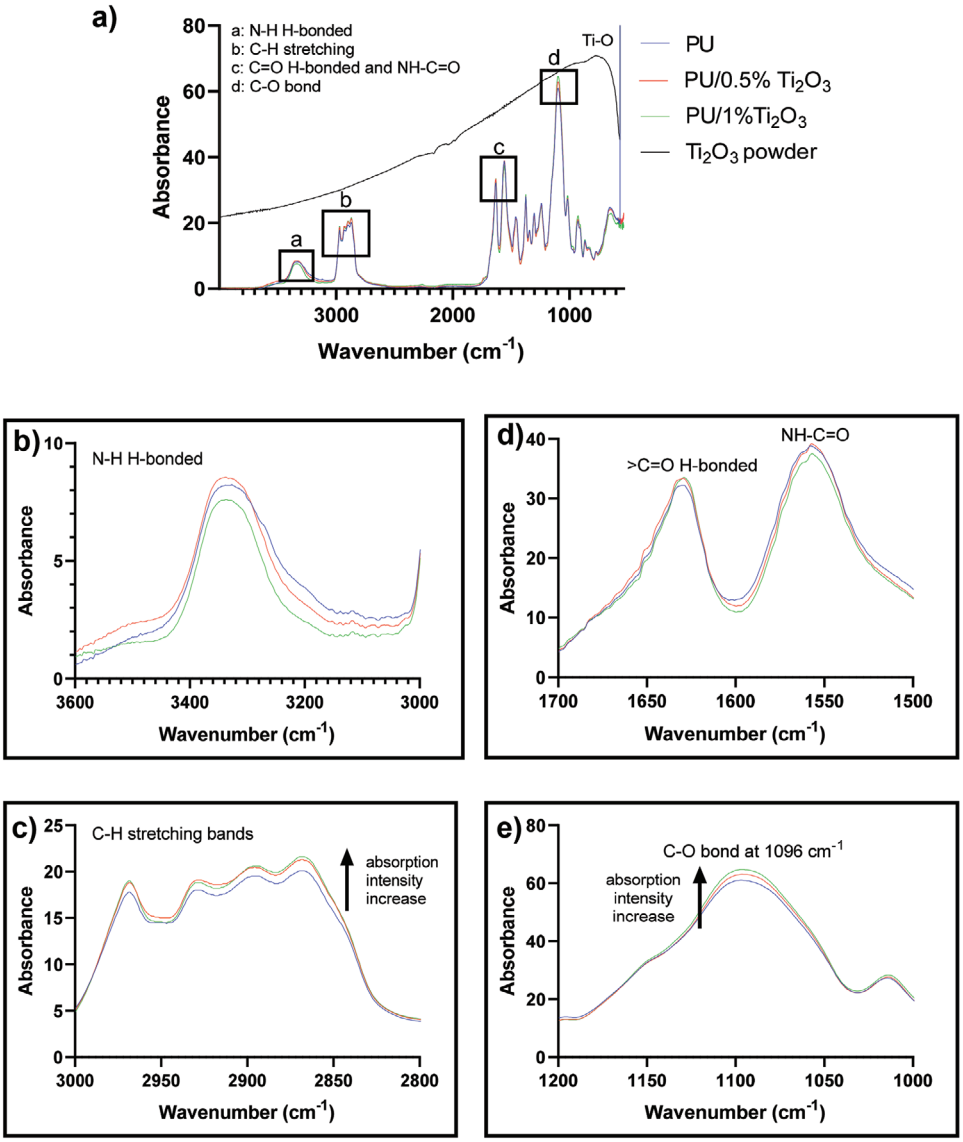

Figure 4. Superimposed FTIR spectra of PU with different loadings of Ti_2O_3, a) full spectra, b) N–H H-bonded region, c) C–H stretching region, d) carbonyl H-bonded region, e) ether, C–O bond region.

of free NH, disordered NH, and disordered C═O in Figure 3b,d suggest that the PU chains are crosslinked via bidentate hydrogen bonding, which will provide high tensile strength. This is supported by He et al.[62] who stated that high hydrogen bonding in HSs could lead to a greater extend of microphase separation in PU which could affect the ultimate mechanical properties.

The presence of silica oxide, NS can be detected at the peaks near 1085 cm^{-1} attributed to the asymmetric stretching vibrations of the Si–O–Si bond and 820 cm^{-1} attributed to the Si–OH bond stretching shown in the entire spectra.[63] It is crucial to point that in this study, a high PU index formulation is used whereby the excess NCO groups could react with the Si-OH group on the silica oxide surface forming a C–O bond. Therefore, as NS content increases, the Si–O–Si or C–O peak absorbance increases. Increasing loadings of silica oxide also gave rise to the absorbance at NH bonded and CO bonded peaks (3327 and 1630 cm^{-1}, respectively). The increase in NH-bonded and C═O bonded peaks could be attributed to the bonded –OH groups stretching vibration[64] indicating the formation of hydrogen bonding with urea groups. The right shift of the ordered carbonyl bond towards a lower wavelength is indicative of the narrower distribution and stronger hydrogen bonding with increasing NS content.[29] The absorbance of ordered carbonyl for PU/1% NS is the highest and has the sharpest peak suggest that 1% NS loading would increase the mechanical properties of PU significantly. From the FTIR curves, it is indicative that the polymer-filler interaction between the OH groups and the functional groups of HSs in PU is enhanced with the increased content of NS particles.

The FTIR spectra of the Ti_2O_3 filled PU (**Figure 4**a) showed an increase in absorption peaks of CH stretching bands (Figure 4c) and aliphatic ether, C–O stretching (Figure 4e). However, these

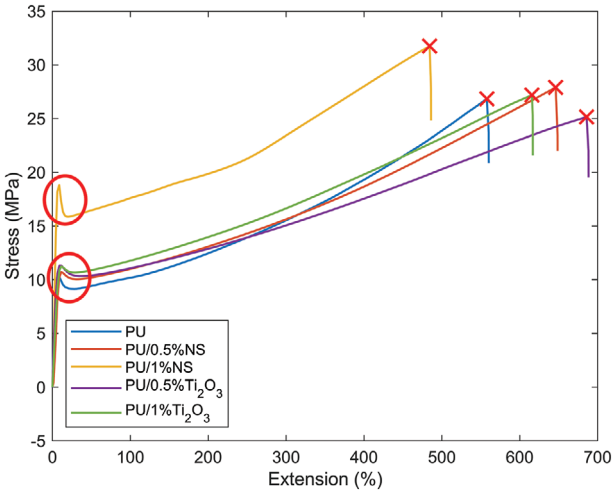

Figure 5. Stress–strain curves of PU and PU composites at 0.5% and 1% filler loadings for the highest tensile strength from each composition; red circles indicate the yield point phenomena at different stress values for different samples; red crosses indicate the fracture point.

peaks do not correspond to the characteristic bond peak of Ti–O which occurs at 776 cm^{-1}. As such, the increase in the peaks corresponding to these bonds indicates that Ti_2O_3 particles are disrupting the SS chain mobility. At 1% Ti_2O_3 loading, the absorption of N–H bonded, C═O bonded and NH–C═O bond peaks (Figure 4b,d) are lower than the neat PU. This could be due to inhomogeneity of Ti_2O_3 dispersion in PU matrix causing agglomeration of these particles. Consequently, the agglomerated Ti_2O_3 are preventing the formation of hydrogen bonds between adjacent urea linkages. For stronger interaction of Ti_2O_3 with PU, surface functionalization of Ti_2O_3 would be a great alternative as it would increase the vicinity of urea groups.[65]

3.3. Mechanical Properties

The stress–strain curves of PU and PU composites in **Figure 5** show that the material experienced elastic deformation going through yield drop (red-circled on the curve) with large plastic deformation afterwards. The yield drop phenomena are followed by strain hardening (a rapid increase of stress) is usually observed for viscoelastic materials.[66] It is noticed that the yield drop for PU/1%NS is rather higher compared to other samples. At the yield point, the force required to overcome the dislocation is lesser than the force required to stretch the atomic bonds resulting in a lower yield point. For PU/1%NS, the yield point is the highest as greater stress is required to overcome the dislocation caused by the silica oxide particles due to their strong interaction with the HS of PU.

From the average tensile strength and elongation bar charts in **Figure 6**a,b, the neat PU sample achieved an average tensile strength of 26.18 MPa and an average elongation of 525%. The *p*-values obtained for each composite sample tabulated in Table S5, Supporting Information, show that most of the samples passed the confidence tests by exhibiting significant values with respect to the neat PU for both tensile and hardness tests. From what is known and reported about the presence of hard and SSs and their contribution to the strength and flexibility of the PU, an increase in HS content will increase the degree of order in the system, however, making the polymer less flexible thus resulting in a decrease in elongation at break. Past studies on aliphatic PU reported low tensile strength values owing to a high concentration of SS.[28,67] Besides, IPDI is regarded as loosely packed isocyanates allowing easy diffusion of HSs into the soft phase.[56] In this study, a high concentration of aliphatic isocyanates (high isocyanate to amine ratio) allowed a higher diffusion rate into the soft phase leading to restriction of polyetheramine chains movement. Restricted chain movement requires high energy to overcome the intermolecular forces which translate to the high tensile strength for the neat PU.

The trend in the tensile strength of the filled PU can be described by the interaction mechanism brought by the fillers into the matrix. The average tensile strength for PU/0.5%NS did not change significantly (*p*-value of 0.3182) as at this loading, there are insufficient silanol, Si–OH groups available for the interfacial interaction with the urea groups to form hard domains. However, at 1% loading of NS, the tensile strength increased significantly by 4 MPa compared to neat PU with a *p*-value of less than 0.0001. The high concentration of NS increased the interfacial interaction between the nanoparticles and urea groups via hydrogen bonding contributing to the increase in hard domains in the PU matrix. This phenomenon is also supported by the stress-strain curve of PU/1%NS (Figure 5). Due to the elastomeric behavior of PU, after the yield point, the chains undergo strain hardening whereby the hard domains are broken down.[68] In the stress–strain curve of PU/1%NS, the strength to overcome the applied load after the yield point is the greatest compared to other samples. The influence of silica oxide on the strength of PU is compared to a study by Pakula et al.[29] who reported a slight increase (up to 2 MPa) for 4% silica oxide loading from their reference aromatic (MDI) based PU. Typically, aliphatic diisocyanates provide less steric hindrance than their aromatic counterparts at the surface of the filler.[42] Thus, this allows the aliphatic urea groups to adopt a spatial orientation, in which carbonyl groups could direct towards silica oxide surface and form not only one but bidentate hydrogen bonds with the Si-OH groups. As for the PU/ Ti_2O_3 samples, the average strength decreased for 0.5% loading with a *p*-value of 0.0242 but did not change significantly for 1% loading in reference to neat PU. The microsized particles are acting as physical barriers for the nano-scaled hard segments to cross-link, and at higher loading, the particles tend to agglomerate leading to inhomogenous dispersion of Ti_2O_3 in the matrix. Due to the agglomeration, PU chains which are not affected by the disturbance of the microparticles tend to cross-link and form hard domain. This shows an inconsistency when microfiller is added into PU.

The change in elongation at break for the filled samples can be described by the chain entanglement of PU. The average elongation at break improved by 18% for PU/0.5%NS but reduced insignificantly for PU/1%NS. The presence of Si–OH groups on the surface of the nanoparticles may cause repulsion towards the ether, C–O groups in SSs, forcing an alignment of PU chains. This favors easier slipping of the chains which is not experienced when the NS loading is increased as the increase in hard domains creates greater entanglement of the chains, restricting their movement during loading. Interestingly, the

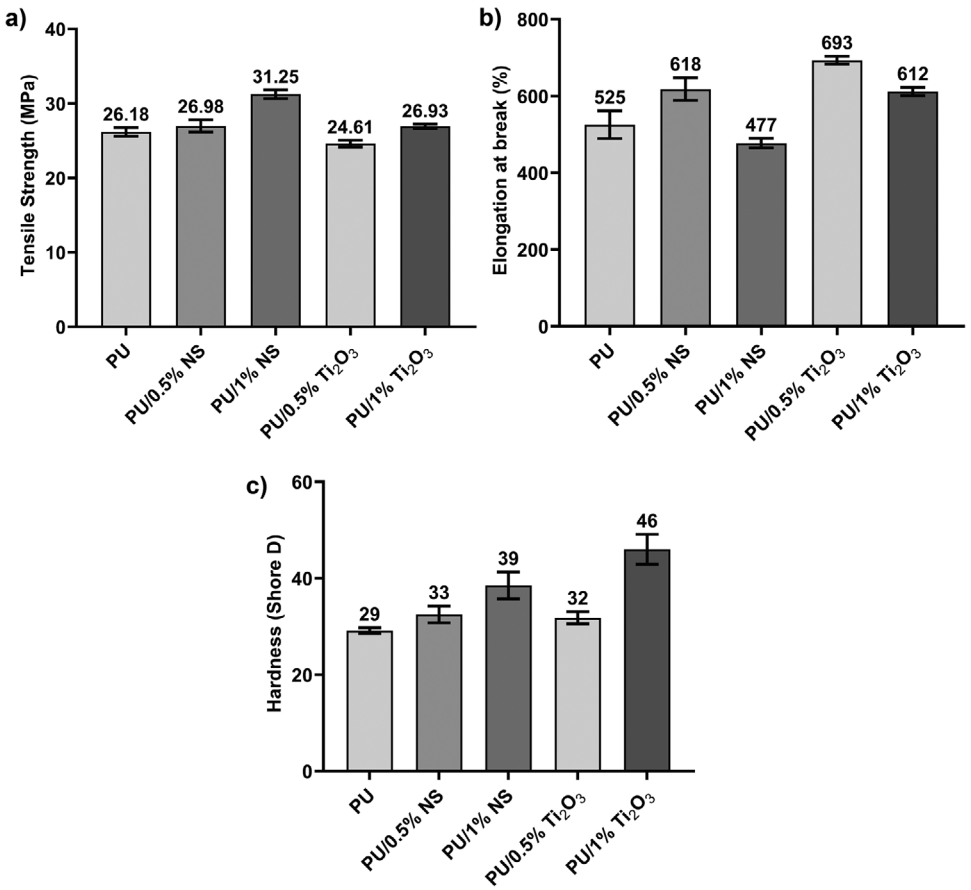

Figure 6. Mechanical properties of PU and PU composites; **a)** average tensile strength, **b)** average elongation at break, **c)** Shore D average hardness.

elongation of PU/0.5% Ti_2O_3 is almost twofold the elongation of PU/0.5% NS with a *p*-value of less than 0.0001. It can be seen that the size of the filler has large influence on the extent of PU chain entanglement. Since the microparticles are occurring as barriers to chain crosslinking and reducing the hard domains, the obstruction is actually forcing the PU chains to align to the stretch direction.[69] While the chain alignment could happen due to the low loading of Ti_2O_3 during the polymerization itself, the PU chains also tend to align during stretching upon breakage of hard domains. The breakage of hydrogen bonding between hard domains and aligning the chains further delays the fracture for PU/0.5% Ti_2O_3. Consequently, when the Ti_2O_3 concentration increases, some particles agglomerate which caused irregularities in the matrix where there are lumps and free space. Such irregularity results in some of the agglomerated particles that orient the chains in the stretch direction as well as some free space for PU chains to entangle with each other. Due to these mixed phenomena occurring concurrently in the PU matrix, the elongation of PU/1% Ti_2O_3 loading is still higher than neat PU.

Indentation resistance is an important material evaluation parameter for measuring its surface performance. From Figure 6c, a general trend of increase in the surface hardness of PU composite is observed with increasing filler loadings. The increased hardness with increasing NS content could be attributed to the thermal curing of the films which changed the distribution of Si–OH bonds by transforming the bonds to Si–O–Si bonds in the PU nanocomposites.[70] Past studies have confirmed that Si–O–Si bonds can easily migrate to the film surface during the curing process and form a dense Si–O–Si network structure, leading to excellent mechanical properties.[71] The most significant improvement in hardness of PU composites in this study is attributed to 1% Ti_2O_3 loading with a p-value of less than 0.0001. The increasing resistance to indentation with higher Ti_2O_3 content could be due to the higher migration of these particles to the film surface during the curing process. Past studies have also reported that oxidation of Ti–O binary oxides during thermal curing increases their shear and Young moduli as well as the hardness owing to their stiffer crystal structure.[72]

3.4. DSC Analysis

In regard to the significant improvement in tensile strength by 1%NS and elongation by 0.5% Ti_2O_3, DSC was used to study the effect of these fillers in the chain mobility of PU. The DSC heating scans in **Figure 7** exhibit the varying glass transition temperatures, T_g with different fillers. The glass transition temperature of the major amine component, polyether D2000 has been reported to be −67 °C,[56] which is much lower than the T_g of neat PU (−46.64 °C) obtained from this study. This result suggests that the HS mainly consisting of urea linkages are loosely packed allowing easy diffusion into the soft domain. This diffusion leads to

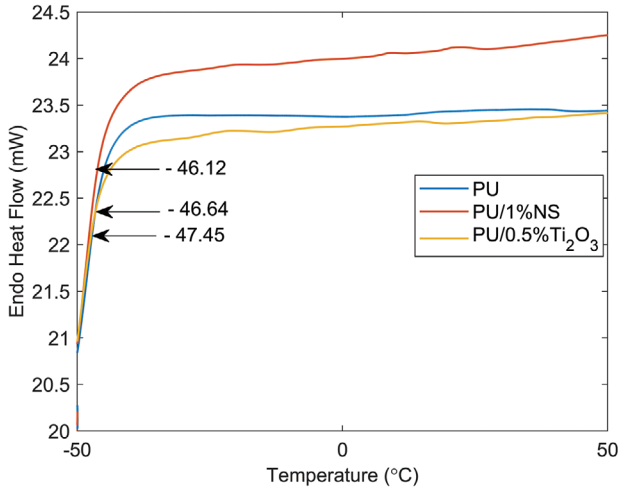

Figure 7. DSC heating scans of PU, PU/0.5% Ti_2O_3, and PU/1% NS from −50 to 50 °C.

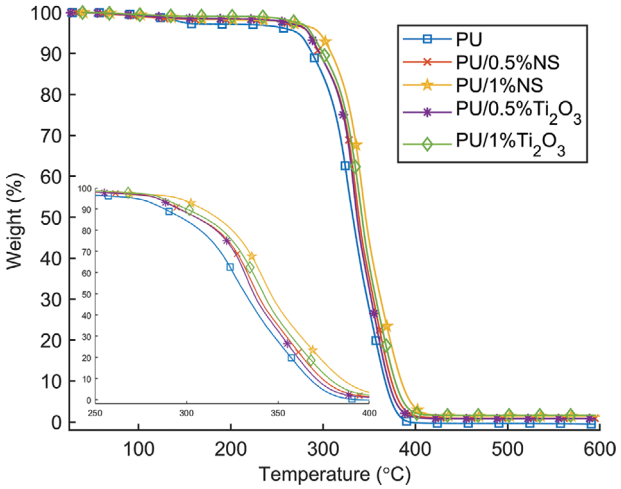

Figure 8. TGA curves for PU and PU composites showing degradation with increasing temperature. Inset: Magnified image of the graph at the degradation range.

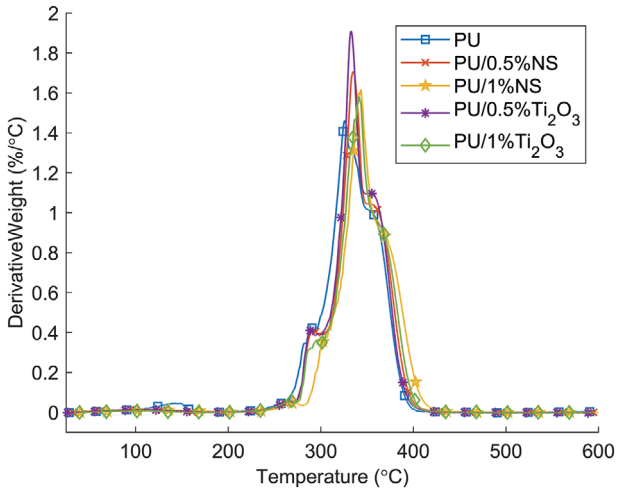

Figure 9. DTG curves for PU and PU composites showing degradation rate with increasing temperature.

restricted chain mobility and slows down the segmental dynamics of polyetheramine chains.[73] The diffusion was possible due to the significant concentration of isocyanate components near the phase boundaries whereby the PU index is 2.77.

The T_g of PU/0.5% Ti_2O_3 was reduced to −47.45 °C, which increased the chain mobility and segmental dynamics of the amine chain leading to improved flexibility. Greater chain mobility in two-phase polymers is a crucial factor in enabling healing abilities,[74] implying that the use of Ti_2O_3 in PU could be an alternative to fabricate self-healable PU in the future. On the other hand, the T_g of PU/1% NS increased to −46.12 °C, which explains the high tensile strength owing to greater restriction in chain mobility by HSs. Another observation that strongly supports this result is the high endothermic heat flow with increasing temperature indicating greater amount of energy required to overcome the intermolecular and polymer-filler forces.

3.5. TGA Analysis

The TGA analysis of neat PU and PU composites in **Figure 8** shows that all the samples have similar weight loss curves. The degradation range starts from 250 °C and stops at around 400 °C. The neat PU began to release its volatile product at 180 °C; below the degradation temperature range (refer to the inset), suggesting that hydrocarbon chains from IPDI or Jeffamine D230 had decomposed due to their lower flashpoints (120 to 155 °C). It has been reported that the degradation steps of segmented PU are attributed to the hard and SSs.[30] The first degradation temperature is a consequence of the low thermal stability of urea bonds in the HS whereas the second degradation temperature is associated with the SS decomposition. Following that, it has been suggested that the amount of weight loss at each degradation stage may be used as a quantitative measurement of the hard and soft content in the sample.[75] However, there is only one distinct degradation peak for all the samples observed from derivatographic (DTG) curves (**Figure 9**). The control sample experienced a peak at 326 °C with 40% mass loss and it slowly shifted to a higher temperature with increasing filler loadings. As the stoichiometry HS in this study is 36.48%, the degradation peak at 326 °C could be from HSs. Consequently, the slight right shift of DTG curves to a higher temperature for maximum degradation rate indicates enhancement of thermal stability with the presence of silica oxide and Ti_2O_3 particles.

From **Table 2**, the highest degradation temperature at both T_{10} and T_{50} were obtained at 1% silica oxide loading from 288.3 to 309 °C (21 °C increments) and 332.3 to 346.1 °C (14 °C increments), respectively. These increment values are higher than observed from the addition of graphene oxide sheets in IPDI-based aliphatic PU, as reported by Qian et al.[28] This shows that 3D nanoconfined particles have improved the thermal stability of PU as compared to 2D nanosheets. PU/1% NS also contributed to the highest char residue in this study with 3.41 wt% char, followed by PU/1%Ti_2O_3 with 2.17 wt%. At both 0.5% and 1% loadings, PU-NS composite left more char residue than PU-Ti_2O_3 composites. This could be due to the nanoscale confinement of silica oxide particles contributing to more vital PU-filler interaction as well

Table 2. TGA properties of PU and its composites with different loadings of silica oxide and titanium (III) oxide from TGA and MTGA experiments.

Sample	Filler loadings [%]	Temperature at 10% mass loss [°C]	Temperature at 50% mass loss [°C]	Char residue at 400 °C [wt%]	Activation energy, E_a [kJ mol^{-1}]
PU	0	288.3	332.3	0	145 ± 15
PU/0.5%NS	0.5	296.3	338.8	1.48	149 ± 19
PU/1%NS	1.0	309.0	346.1	3.41	170 ± 16
PU/0.5%Ti_2O_3	0.5	296.1	336.8	1.13	195 ± 15
PU/1%Ti_2O_3	1.0	300.3	342.1	2.17	180 ± 19

as weak adhesion between PU matrix and Ti_2O_3 particles. High char yield is essential to provide a thermal insulating layer while the polymer is burning which is helpful to lower the temperature of the PU surface beneath the char.[30] This suggests that silica oxide brings a better flame-retardant property to PU as compared to Ti_2O_3.

Provided that the temperature at the onset of the degradation process is affected by the fillers, a more accurate evaluation of the thermal stability can be drawn by kinetics analysis, and in particular, considering the activation energy, E_a. Activation energy is the energy required for polymer to move from one location to another. This approach was succeeded in the characterization of composite materials using modulated TGA analysis (mTGA).[76,77] An increase in E_a is observed for NS-filled composite at increasing filler concentration attributed to the strong interaction of the silanol group on the nanoparticles and the NH–CO in the urea linkage. The strong interaction immobilizes the PU chains, hence requiring greater energy with increasing concentration of silica oxide for the breakage of the hydrogen bonding within the hard domains. A similar enhancement of E_a was observed in a previous study on nanoclay-polyurethane composites where the addition of 3 wt% improved the E_a by 25%.[78] In this study, Ti_2O_3 improved the E_a of PU much higher than nanosilica oxide owing to their larger size. Unsurprisingly, the E_a trend of PU/ Ti_2O_3 is similar to its trend of elongation at break whereby the Ea increased at 0.5% Ti_2O_3 loading by 35% and dropped slightly at 1% loading. However, addition of Ti_2O_3 did enhance the E_a of PU at both the loadings. This is because, Ti_2O_3 microparticles are existing as physical barrier and adhering to the PU chains, which obstructs the movement of the chains. At 0.5% loading, the obstruction is more regular throughout the matrix, providing shielding as well as stiffening effect to the chains and hindering the formed gases from thermal decomposition of PU to penetrate the gaps of the matrix. At 1% loading however, some agglomeration of the Ti_2O_3 led to some PU chains unshielded by the microparticles exposed to the formed gases resulting in slight drop in the E_a value.

3.6. Dynamic Mechanical Analysis (DMA)

The viscoelastic properties and the interfacial interaction of filled PU were investigated using DMA experiments under an oscillatory regime. **Table 3** reports the rheological parameters at 30 °C for neat PU and PU composites with increasing amounts of filler (NS and Ti_2O_3). The storage modulus refers to the ability of the material to store energy while going through deformation.

Table 3. Rheological parameters of PU based materials at 30 °C.

Sample	Storage Modulus [MPa]	Loss Modulus [MPa]	tan(δ)
PU	2.224	0.2547	0.1145
PU/0.5% NS	6.749	0.5939	0.0879
PU/1% NS	2.238	0.2285	0.1021
PU/0.5% Ti_2O_3	2.754	0.2774	0.1007
PU/1% Ti_2O_3	8.629	0.7302	0.0846

As a general result, the addition of the filler induced the decrease of tan(δ), indicating that the elastic component was enhanced in the nanocomposite materials compared to that of the pure polymer. In particular, it was observed that the presence of 1% of Ti_2O_3 conferred the highest storage modulus with 288% improvement from the neat PU. Interestingly, similar viscoelastic characteristics were observed for PU/0.5% NS. In this regard, it should be noted that the further addition of NS particles (1%) generated a slight increase in the tan(δ) value, however, no significant change was observed in the storage and loss moduli. This could be attributed to the inhomogeneity of the silica oxide dispersion in PU due to increased viscosity at this loading. The increasing loss modulus values (except for PU/1%NS) result from friction between the fillers and PU chains resulting in high dissipation of energy. At the same time, higher chain mobility increases the internal friction between the polymer chains. The peak values of tan (δ) indicate the internal friction of the polymer chains.[79] The reduction in tan (δ) as filler concentration increases indicate a reduction in internal friction between the PU chains. This suggests that a robust interfacial interaction is established between the fillers and PU chains.

DMA tests were conducted by heating the samples to explore the effects of the temperature on the viscoelastic behavior of PU-based materials. Within this, **Figure 10** compares the dependences of storage (G′) and loss (G″) moduli on temperature for neat PU and PU composites containing 0.5% of filler. It was observed that all the samples presented a sigmoidal decreasing trend for the G′ versus temperature plot. On the other hand, G″ evidenced a peak within the temperature interval between 100 and 140 °C that can be related to the order-disorder transition of PU.[30] It was estimated that the temperatures at the G″ maxima as $T_{max\text{-}G''}$. The obtained values (**Table 4**) evidenced that the addition of NS (1%) and Ti_2O_3 (0.5% and 1%) shifted the PU transition to lower temperatures (left shift) to that of the pure polymer. The left shift for PU/Ti_2O_3 could be related to the FTIR result ob-

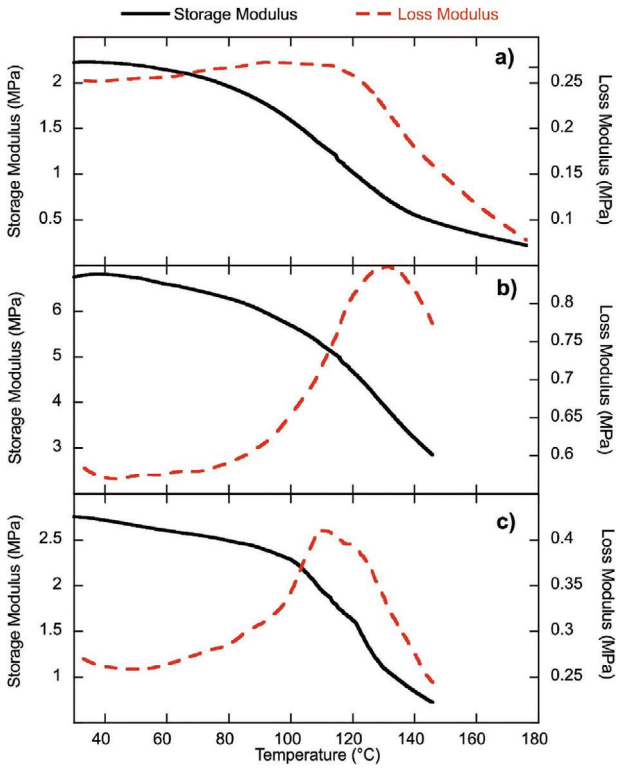

Figure 10. Storage modulus (solid black line) and loss modulus (slashed red line) as functions of temperature for a) PU, b) PU/0.5% NS, and c) PU/0.5% Ti_2O_3.

Table 4. Transition temperatures determined from DMA experiments.

Sample	$T_{max\text{-}G''}$ [°C]	$T_{ons\text{-}tan(\delta)}$ [°C]
PU	113.0	102.8
PU/0.5% NS	130.2	106.4
PU/1% NS	107.4	93.9
PU/0.5% Ti_2O_3	109.5	98.5
PU/1% Ti_2O_3	111.8	98.9

tained for the decreasing carbonyl and NH bonded peaks, which indicates lower PU-Ti_2O_3 friction during stretching. The sandwich sample with inhomogeneous dispersion of silica oxide at 1% loading could have contributed to the left shift of the temperature. Interestingly, the opposite effect was detected for the PU/0.5% NS indicating a strong interaction between PU and silica oxide leading to difficulty in chain mobility during stretching. As shown in **Figure 11**, the PU transition can be detected by the increase of tan(δ) occurring at ≈100 °C. Accordingly, the transition temperatures are calculated from the onset ($T_{ons\text{-}tan(\delta)}$) of tan($\delta$) versus temperature function. $T_{ons\text{-}tan(\delta)}$ values (Table 4) are in agreement with the previous discussion concerning the $T_{max\text{-}G''}$ data.

3.7. Surface Morphology

From the FE-SEM of PU and PU composites' surfaces shown in **Figure 12**, the PU surface shows a relatively smooth surface in-

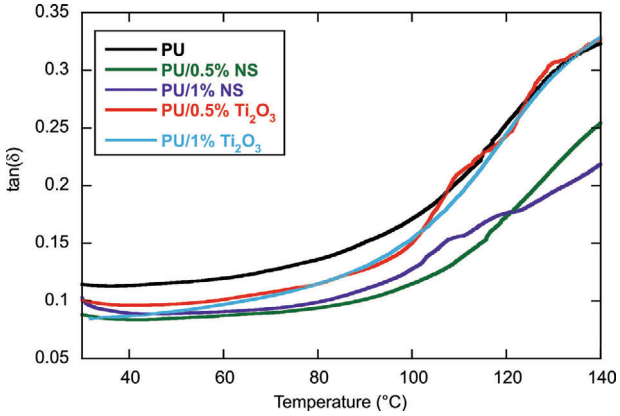

Figure 11. Tan(δ) as a function of the temperature for pristine PU and PU-based nanocomposites.

dicating a good homogeneity. The PU/1% NS shows some lines along a slightly rough surface indicating a good dispersion of the NS particles within the matrix. On the other hand, on the PU/1% Ti_2O_3 surface, there are white coarse particles present in irregular dispersion, indicating an agglomeration of the Ti_2O_3 fillers in the PU matrix.

From the cross-sections of tensile fracture specimens in **Figure 13**, a long fracture line (continuous laminate) is observed on the neat PU accompanied by crazing lines at the edge (Figure 13a). Crazing occurs due to the stretching of the molecular network while resisting stress and elongation during tensile loading. At a closer look at the fracture line, the surface exhibits orderly fish striated muscle-like structure, similarly observed in past studies.[28,80] There is a significant stretching line (Figure 13b) creating phase separation due to the viscous flow of PU during its curing. At 10.0k magnification, some dimples are also visible which could have acted as stress concentrators. Though the pin-hole dimples attributed to the fracture, their nanoscale size demonstrated that there was a good mixing of PU solution during the synthesis step. In the case where they are in a microscale, the stress concentration would be higher, resulting in lower strength. The gelling effect of viscous PU is more prominent as thicker stretching lines are seen on the PU/1%NS fracture surface (Figure 13d). The craters seen in Figure 13e could be due to the encapsulations of NS by the viscous PU. These craters are filled with dispersed particles sticking on the walls (Figure 13f) indicating that the nanosilica oxide particles have successfully adhered and formed interfacial interaction with the PU matrix. In contrast to PU and NS filled PU fracture surfaces, the hole at the edge on PU/1%Ti_2O_3 exhibits fibrous structure strongly indicating ductile fracture. This observation supports the 17–32% increment in the elongation at break of PU with addition of 0.5% and 1% Ti_2O_3. Irregular micro-sized particles are clustered with each other in the matrix and these particles are confirmed to be Ti_2O_3 particles as shown in Figure S2, Supporting Information.

Both the composite fracture surfaces have very rough surfaces compared to the smooth neat PU fracture surface. One possible reason is after fracture, a soft phase layer reassembles to cover the surface of neat PU because the soft phase has a lower surface energy and a low T_g.[81] To minimize the surface area, this

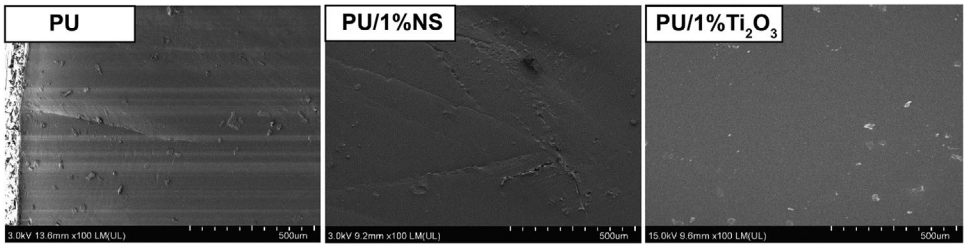

Figure 12. Micrographs of PU and its composites before tensile fracture at 100× magnification under FE-SEM.

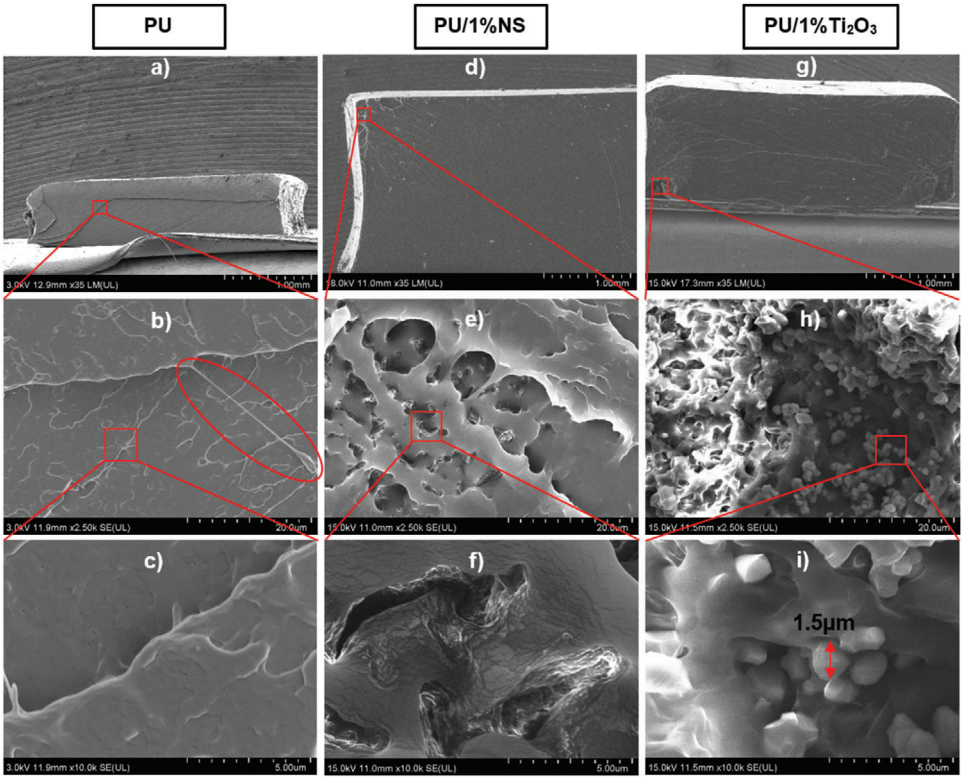

Figure 13. Micrographs of tensile fractured cross-sectional surfaces of PU (a–c), PU/1%NS (d–f), and PU/1% Ti_2O_3 (g–i) at low (35×) and high magnifications (2.50k× and 10.0k×) under FE-SEM.

soft-phase surface layer creates a smooth surface. In the composites, however, the soft phase cannot cover the surface efficiently as the fillers disrupted the phase separation in PU and were driven by the interfacial interaction formed by the fillers with PU matrix.

3.8. XRD Analysis

XRD analysis was performed to identify the changes in the crystallinity structure of PU with the addition of 1% NS and 1% Ti_2O_3, respectively. For all the samples as shown in **Figure 14**, a broad scattering peak (peak 2) with maxima centering at $\approx 2\theta = 19°$ contributed by aliphatic diisocyanate (IPDI) in line with other studies,[56,82] confirming the amorphous form of PU. The broad peak suggests that it derives from the loosely packed hard domain by bulky IPDI. The absorption intensity increased with the addition of 1% NS and 1/%Ti_2O_3 for peak 2. This illustrates that the introduction of silica oxide and Ti_2O_3 particles increase the crystallinity of the PU matrix. Ti_2O_3 at 1% loading increased the crystallinity of the PU matrix higher than silica oxide at the same loading. However, the tensile strength at 1% Ti_2O_3 loading is about 5 MPa lower than that of at 1% NS loading. Increased crystallinity leads to a more ordered structure which increases the tensile strength of the material. In the case of large molecular weight polymer like PU, greater entanglement of polymer chains occur due to higher crosslinking density as a result of increased crystallinity, and the intermolecular bonding increases with increased crystallinity.[83]

Table 5 lists the characteristic peaks experienced by the samples are displayed and the d-spacing was calculated using Equation (1). The interdomain spacing (d) represents the distance between neighboring hard domains. The interdomain spacing

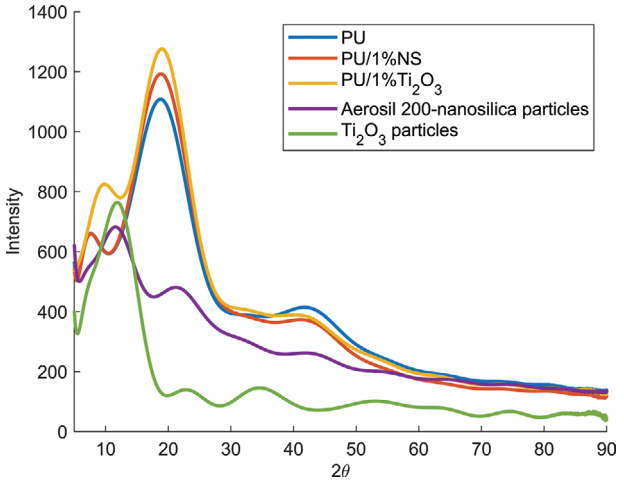

Figure 14. Smoothened XRD profiles of PU, PU composites, and untreated fillers; NS and Ti_2O_3.

Table 5. 2-Thetas and d-spacing from XRD profiles of PU and PU composites.

Sample	2-theta			d-spacing [nm]		
	Peak 1	Peak 2	Peak 3	Peak 1	Peak 2	Peak 3
PU	7.5	18.8	42.5	0.13	3.11	0.11
PU/1% NS	7.5	18.8	42.2	0.13	3.11	0.09
PU/1% Ti_2O_3	9.7	18.9	42.0	0.07	3.05	0.09

remains unchanged after the addition of 1% NS to the neat PU, however, it decreased after adding 1% Ti_2O_3. Decreasing d-spacing indicates less efficient hard segmental packing[84] and weaker intermolecular forces.[85]

According to the XRD and mechanical tests analysis, it shows that the PU chains in PU/1% Ti_2O_3 are more loosely packed incurring lower strength but at the same time they are regularly aligned which led to higher hardness. It appears that larger sized filler loosens the packing of hard domains in the PU matrix than smaller-sized fillers. XRD results also suggest that Ti_2O_3 brought a higher degree of order in the matrix as compared to silica oxide. Loosely packed hard domain aids in the chain mobility during loading and unloading leading to higher elongation at break whereas tightly packed hard domain requires greater force to disentangle the polymer chains leading to greater strength. A combination of Ti_2O_3 and silica oxide in an aliphatic PU matrix would give a balanced hard domain packing and optimum strength and elongation at break.

3.9. Surface Wettability

The water contact angle of PU and PU composites surface decrease with time for 270 s as shown in **Figure 15**a. This could be explained by the possible presence of impurities in the water on the localized surface with caused the smaller angle.[86] Other than that, local nano- or micro-particle concentrations in the sample may also contribute to the decrease in water contact angle over time.[86] From the analysis of kinetic evolution of the water contact angle, the experimental water contact angles were fitted by the empirical Equation (2) and the kinetic constants are presented in **Table 6**. The experimental data follows the contact angle evolution trend by the empiric showing that this equation fits to evaluate contact angle evolution on PU composites. The curve fitting is crucial to evaluate the water droplet spreading contribution, n by the fillers in the films.[87]

Neat PU film showed hydrophilic behavior with an initial contact angle of 75°. It is expected that filled PU will exhibit higher water contact angles. As such, if the fillers are dispersed well in the polymer matrix, strong interaction between fillers and polymer will decrease the surface energy thus making the surface more hydrophobic.[88] The NS-filled PU increased the hydrophobicity of the PU surface at both 0.5% and 1% loadings. The hydrophobic effects by 1% NS loading in PU are compared with neat film in Figure 15b. Though both loadings had large contact angles initially and the spreading process rate (k_θ) increased, only 1% NS-filled PU surface remained more hydrophobic than the neat PU throughout. This indicates the surface energy at the localized region on PU/1%NS is the lowest of all samples in this study supported by the increase in spreading contribution, n. The hydroxyl groups around silica particles interacted with urea groups which possibly brought the PU matrix a higher degree of order as confirmed by tensile and FTIR results. This interaction possibly decreased the polar OH groups available to water on the surface which increased the contact angle.

Ti_2O_3 particles are known to exhibit hydrophilic behavior when in contact with water molecules.[89] Thus, in general, the contact angles of PU/Ti_2O_3 at both loadings remained lower than the neat PU surface. This is due to the adsorption energy of H_2O on the Ti_2O_3 filled PU surfaces being lower as compared to the neat PU itself. Thus, to improve the hydrophobicity of PU, silica oxide is a better candidate than Ti_2O_3.

3.10. Interaction Mechanism

Figure 16 shows the schematic of overall interaction mechanism in the neat PU and the PU composite samples proposed based on the findings of this study. The interaction between the urea, NH-CO groups results in the formation of bidentate or monodentate hydrogen bonding, which makes up the hard domains (Figure 16a). The formation of these hard domains leads to entanglement of the soft segmental chains resulting in restriction in motion during stretching. The addition of silica oxide (NS) nanoparticles and titanium (III) oxide (Ti_2O_3) microparticles changes the overall structure, packing, and dynamics of the PU matrix as shown in Figure 16b,c, respectively.

NS particles interact with each other via weak Van der Waals' forces which could be dominant in high concentrations leading to formation of aggregates. At low NS loading, the elongation of PU was seen to be enhanced greatly possibly due to the dominating interaction between negatively charged OH groups of the nanoparticles. Furthermore, the addition of NS into PU leads to strong interaction between the silanol, Si–OH bonds, and the NH–CO groups via formation of bidentate hydrogen bonding. This interfacial interaction is largely influenced by the easy adoption of spatial orientation by the bulky aliphatic diisocyanate (IPDI). By forming hydrogen bonds, they contribute to the for-

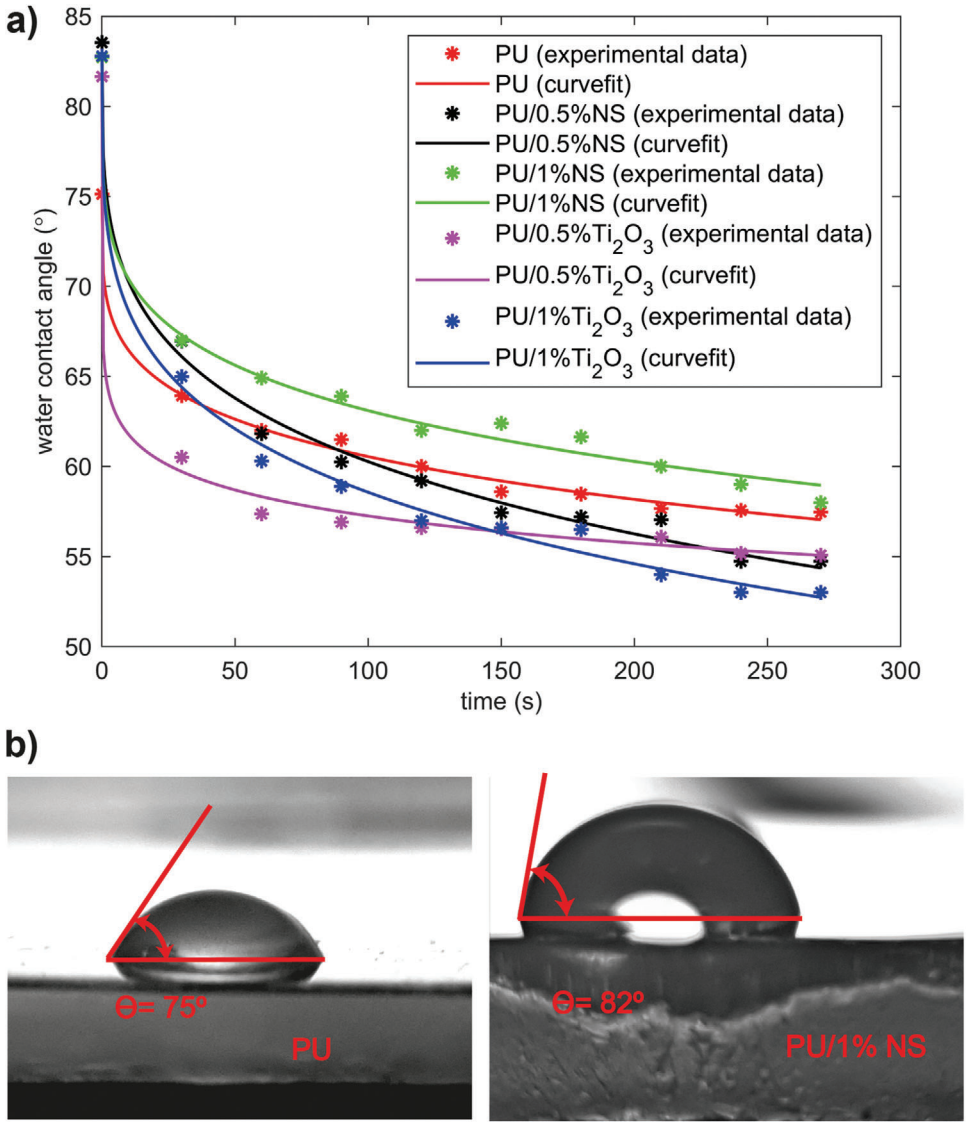

Figure 15. a)Water contact angle tests for a period of 270 s for PU composites, b) Images of water droplets just after their deposition on the surfaces of PU and PU/1%NS.

Table 6. Water contact angle kinetic constants of PU and PU composites.

Sample	k_θ [s^{-1}]	n
PU	0.0696 ± 0.0049	0.2455 ± 0.0139
PU/0.5%NS	0.0914 ± 0.0094	0.2763 ± 0.0200
PU/1%NS	0.0957 ± 0.0088	0.2856 ± 0.0180
PU/0.5%Ti_2O_3	0.2190 ± 0.0162	0.1048 ± 0.0146
PU/1%Ti_2O_3	0.1013 ± 0.0090	0.2667 ± 0.0174

mation of hard domains and chain entanglement, which further obstruct the chain motion during stretching. This interaction is mostly noticeable in PU/1% NS as higher concentration of the nanoparticles provides greater interfacial area resulting in the significant increase in tensile strength, thermal stability, storage modulus, and water contact angle in PU/1% NS.

The interaction mechanism in PU/Ti_2O_3 matrix appears merely physical with PU and electrostatic intermolecular forces between the Ti_2O_3 particles. The presence of the microparticles between PU chains hinders the chains to cross-link, by acting as physical barriers. Their presence between the chains results in a more orderly structure, as seen in the enhanced crystallinity of PU in the XRD analysis. At the same time, the particles provide space to the PU chains to relax due to their larger size. This phenomenon explains the increase in elongation (higher than neat PU) but decreases in the tensile strength. Moreover, the cluster formation of Ti_2O_3 also resulted in the decrease in water contact angle which led to a more hydrophilic surface over time as compared to neat PU. Subsequently, increasing concentration of Ti_2O_3 beyond 0.5% resulted in two phenomena; one is the ionic nature of the microparticles which have caused agglomeration and provided free space for PU chain entanglement and two, are some of the microparticles adhere to PU chains and

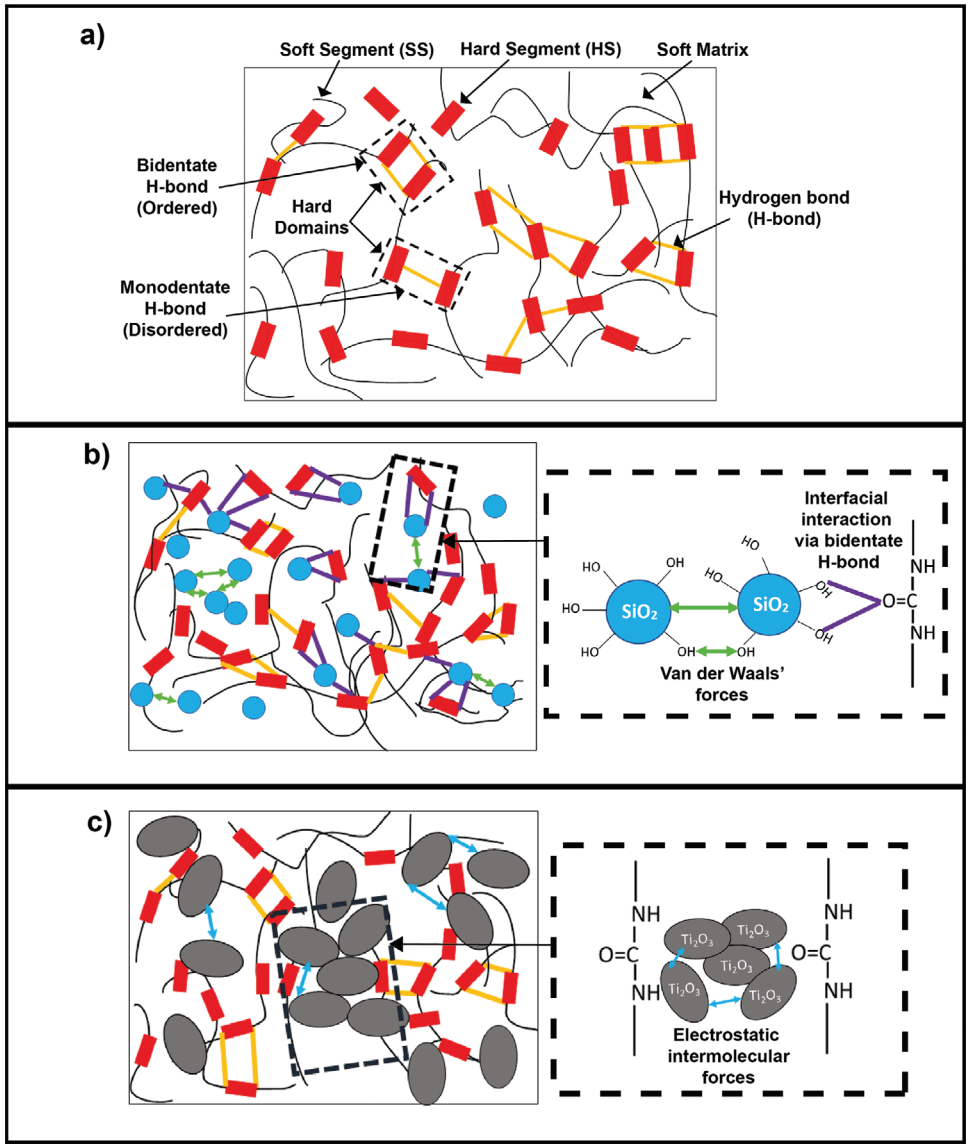

Figure 16. Schematic illustration of the interaction mechanism in neat PU and PU composites; a) neat PU, b) PU with silica oxide (NS), c) PU with titanium (III) oxide (Ti_2O_3).

giving stiffening effect to the chains. These two phenomena occurring concurrently in the matrix are strongly observed in the unchanged tensile strength, increase in elongation, increase in the E_a and increase in the storage modulus.

4. Conclusions

In summary, a solvent-free aliphatic PU with high mechanical, thermal, and rheological properties was prepared. The diffusion of HSs into the soft domain restricted the chain mobility forming tight packing, thanks to the high index of PU in this study. Besides, the inclusion of silica oxide and Ti_2O_3 at low loadings has greatly enhanced the mechanical and thermal performances of PU. The addition of fillers was observed to disrupt the phase separation in PU matrix resulting in craters containing silica oxide nanoparticles and agglomerated Ti_2O_3 particles, respectively. This disruption in PU/NS composite, led to strong interfacial interaction between the silanol and urea groups incurring in a more efficient hard segmental packing and enhancing the thermal degradation performance. The reduction in the OH end groups on the nanoparticles via interfacial interaction with urea moieties effectively improved the tensile strength and improved the hydrophobicity as well. In contrast, the disruption of PU phase separation by crystalline Ti_2O_3 particles brought relaxation to the soft segmental dynamics and regularity to the overall structure of PU by acting as physical barriers between the chains. The high crystallinity and high toughness of Ti_2O_3 particles enhanced the storage modulus, hardness, and thermal degradation performances of PU. The findings of this study, developed a deeper understanding of the influence of the reinforcing fillers in the segmental packing and chain dynamics of PU, giving new insights into the material design. Moreover, the high index and reduction in the

amine viscosity evidently played a crucial role in the interaction of hard and SSs with the fillers. The properties achieved in this study, could open a window for aliphatic PU to be employed as a standalone material in the industry for diverse applications including strong and flexible films for devices and anti-reflective films for PV and electrical applications.

Supporting Information

Supporting Information is available from the Wiley Online Library or from the author.

Acknowledgements

The authors would like to thank the Ministry of Higher Education Malaysia for providing financial support under Fundamental Research Grant Scheme, FRGS/1/2018/STG07/MUSM/02/2, Monash University Malaysia (MUM) for the Ph.D. scholarship, and the technical officers of the School of Engineering (MUM), Mr. Nasrun (tensile testing), Ms. Nur Azreen (FTIR), Mr. Afiq (FE-SEM), Ms. Nurul Hidayah (TGA), and technical officer of School of Science, Ms. Nurul Amirah (DSC) for their kind assistance.

Conflict of Interest

The authors declare no conflict of interest.

Author Contributions

The manuscript was written through the contributions of all authors. All authors have given approval to the final version of the manuscript.

Data Availability Statement

The data that supports the findings of this study are available in the supplementary material of this article.

Keywords

polyurea dynamics, segmental packing, silica oxide, solvent-free polyurea, titanium (III) oxide

Received: August 5, 2021
Revised: September 23, 2021
Published online: November 9, 2021

[1] S. Giraud, S. Bourbigot, M. Rochery, I. Vroman, L. Tighzert, R. Delobel, F. Poutch, *Polym. Degrad. Stab.* **2005**, *88*, 106.
[2] N. Iqbal, M. Tripathi, S. Parthasarathy, D. Kumar, P. K. Roy, *ChemistrySelect* **2018**, *3*, 1976.
[3] R. G. Rinaldi, M. C. Boyce, S. J. Weigand, D. J. Londono, M. W. Guise, *J. Polym. Sci., Part B: Polym. Phys.* **2011**, *49*, 1660.
[4] K. Yao, Z. Liu, T. Li, B. Guo, Z. Zhuang, *Polymer* **2020**, *202*, 122741.
[5] T. El Sayed, W. Mock, Jr., A. Mota, F. Fraternali, M. Ortiz, *Comput. Mech.* **2009**, *43*, 525.
[6] P. Zhang, Z. Wang, P. Zhao, L. Zhang, X. C. Jin, Y. Xu, *Thin-Walled Struct.* **2019**, *144*, 106342.
[7] N. Iqbal, M. Tripathi, S. Parthasarathy, D. Kumar, P. K. Roy, *RSC Adv.* **2016**, *6*, 109706.
[8] N. Iqbal, P. K. Sharma, D. Kumar, P. K. Roy, *Constr. Build. Mater.* **2018**, *175*, 682.
[9] Y.-S. Chen, B. Wang, B. Zhang, Q. Zheng, J.-N. Zhou, F.-N. Jin, H.-L. Fan, *Def. Technol.* **2020**, *16*, 136.
[10] D. Mohotti, M. Ali, T. Ngo, J. Lu, P. Mendis, *Mater. Des.* **2014**, *53*, 830.
[11] E. Zur, *Adv. Mater. Res.* **2010**, *95*, 85.
[12] B. Shojaei, M. Najafi, A. Yazdanbakhsh, M. Abtahi, C. Zhang, *Polym. Adv. Technol.* **2021**, *32*, 2797.
[13] S. Shi, Y. Liao, X. Peng, C. Liang, J. Sun, *Int. J. Impact Eng.* **2019**, *132*, 103335.
[14] L. Rueda-Larraz, B. F. D'arlas, A. Tercjak, A. Ribes, I. Mondragon, A. Eceiza, *Eur. Polym. J.* **2009**, *45*, 2096.
[15] L. Yingjie, W. Kang, J. O. Stoffer, B. Chu, *Macromolecules* **1994**, *27*, 612.
[16] M. A. Corcuera, L. Rueda, A. Saralegui, M. D. Martín, B. Fernández-D'arlas, I. Mondragon, A. Eceiza, *J. Appl. Polym. Sci.* **2011**, *122*, 3677.
[17] Y. He, D. Xie, X. Zhang, *J. Mater. Sci.* **2014**, *49*, 7339.
[18] C. Fang, W. Liu, X. Qiu, *Macromol. Mater. Eng.* **2019**, *304*, 1900257.
[19] S. Sami, E. Yildirim, M. Yurtsever, E. Yurtsever, E. Yilgor, I. Yilgor, G. L. Wilkes, *Polymer* **2014**.
[20] D. B. Klinedinst, I. Yilgör, E. Yilgör, M. Zhang, G. L. Wilkes, *Polymer* **2012**.
[21] M. Tripathi, S. Parthasarathy, P. K. Roy, *J. Appl. Polym. Sci.* **2020**, *137*, 48573.
[22] X. Qian, L. Song, Q. Tai, Y. Hu, R. K. K. Yuen, *Compos. Sci. Technol.* **2013**, *74*, 228.
[23] K. Holzworth, Z. Jia, A. V. Amirkhizi, J. Qiao, S. Nemat-Nasser, *Polymer* **2013**, *54*, 3079.
[24] D. Fragiadakis, R. Gamache, R. B. Bogoslovov, C. M. Roland, *Polymer* **2010**, *51*, 178.
[25] J. M. Sirrine, S. A. Schexnayder, J. M. Dennis, T. E. Long, *Polymer* **2018**, *154*, 225.
[26] B. S. Ritter, R. Mülhaupt, *Macromol. Mater. Eng.* **2017**, *302*, 1600338.
[27] W. C. Pan, K. Liao, C.-H. Lin, S. A. Dai, *J. Polym. Res.* **2015**, *22*.
[28] X. Qian, L. Song, B. Yu, W. Yang, B. Wang, Y. Hu, R. K. K. Yuen, *Chem. Eng. J.* **2014**, *236*, 233.
[29] D. Pakuła, M. Dobrosielska, B. Sztorch, M. Popiół, B. Klonowski, D. Brząkalski, B. Marciniec, R. E. Przekop, *Compos. Theory Pract.* **2019**, *19*, 76.
[30] W. H. Awad, C. A. Wilkie, *Polymer* **2010**, *51*, 2277.
[31] T. Cheng, G. Lv, Y. Li, H. Yun, L. Zhang, Y. Deng, L. Lin, X. Luo, J. Nan, *Macromol. Mater. Eng.* **2021**, *306*, 2100086.
[32] U. Kabariya, S. James, *Vibration* **2020**, *3*, 162.
[33] D. F. Zambrano, R. Villarroel, R. Espinoza-González, N. Carvajal, A. Rosenkranz, A. G. Montaño-Figueroa, M. J. Arellano-Jiménez, M. Quevedo-Lopez, P. Valenzuela, W. Gacitúa, *Sol. Energy Mater. Sol. Cells* **2021**, *220*, 110841.
[34] C. Gao, Y. Z. Jin, H. Kong, R. L. D. Whitby, S. F. A. Acquah, G. Y. Chen, H. Qian, A. Hartschuh, S. R. P. Silva, S. Henley, P. Fearon, H. W. Kroto, D. R. M. Walton, *J. Phys. Chem. B* **2005**.
[35] M. H. Kirmani, P. J. Arias-Monje, S. Kumar, *ACS Appl. Nano Mater.* **2019**, *2*, 6849.
[36] G. Toader, E. Rusen, M. Teodorescu, A. Diacon, P. O. Stanescu, C. Damian, T. Rotariu, A. Rotariu, *J. Appl. Polym. Sci.* **2017**, *134*, 45061.
[37] L. Jiang, Y. Lei, Y. Xiao, H. Xu, A. Yuan, Z. Wei, Y. Chen, J. Lei, *Chem. Eng. J.* **2021**, *410*, 128354.
[38] W. Akl, M. Nouh, O. Aldraihem, A. Baz, *Mech. Time-Depend. Mater.* **2019**, *23*, 223.
[39] R. Casalini, R. Bogoslovov, S. B. Qadri, C. M. Roland, *J. Polym.* **2012**, *53*, 1282.

[40] S. M. Mirabedini, R. R. Farnood, M. Esfandeh, F. Zareanshahraki, P. Rajabi, *Prog. Org. Coat.* **2020**, *142*, 105592.
[41] J.-H. Song, H.-C. Eun, *Civ. Eng. J.* **2021**, *7*, 407.
[42] R. L. D. Whitby, A. V. Korobeinyk, V. M. Gun'ko, D. B. Wright, G. Dichello, L. C. Smith, T. Fukuda, T. Maekawa, J. R. Thorpe, S. V. Mikhalovsky, *J. Phys. Chem. C* **2013**, *117*, 11829.
[43] X. Qian, B. Yu, C. Bao, L. Song, B. Wang, W. Xing, Y. Hu, R. K. K. Yuen, *J. Mater. Chem. A* **2013**, *1*, 9827.
[44] Y. Ma, Y. Zhang, J. Liu, Y. Ge, X. Yan, Y. Sun, J. Wu, P. Zhang, *Mater. Des.* **2020**, *189*, 108547.
[45] S. Mallakpour, M. Naghdi, *Prog. Mater. Sci.* **2018**, *97*, 409.
[46] A. Allahverdi, M. Ehsani, H. Janpour, S. Ahmadi, *Prog. Org. Coat.* **2012**, *75*, 543.
[47] Y.-G. Miao, H.-Y. Liu, T. Suo, Y.-W. Mai, F.-Q. Xie, Y.-L. Li, *Composites, Part B* **2016**, *96*, 119.
[48] G. Polizos, E. Tuncer, I. Sauers, K. L. More, *Polym. Eng. Sci.* **2011**, *51*, 87.
[49] M. Zhang, Y. Li, Z. Su, G. Wei, *Polym. Chem.* **2015**, *6*, 6107.
[50] M. A. Hussein, K. A. Alamry, S. J. Almehmadi, M. A. Elfaky, H. Džudžević-Čančar, A. M. Asiri, M. A. Hussien, *Des. Monomers Polym.* **2020**, *23*, 59.
[51] R. L. Blaine, B. K. Hahn, *J. Therm. Anal. Calorim.* **1998**, *54*, 695.
[52] A. F. Stalder, T. Melchior, M. Müller, D. Sage, T. Blu, M. Unser, *Colloids Surf., A* **2010**, *364*, 72.
[53] S. Farris, L. Introzzi, P. Biagioni, T. Holz, A. Schiraldi, L. Piergiovanni, *Langmuir* **2011**, *27*, 7563.
[54] B. Orel, H. Spreizer, A. Šurca Vuk, M. Fir, D. Merlini, M. Vodlan, M. Köhl, *Sol. Energy Mater. Sol. Cells* **2007**, *91*, 108.
[55] J. Loste, J.-M. Lopez-Cuesta, L. Billon, H. Garay, M. Save, *Prog. Polym. Sci.* **2019**, *89*, 133.
[56] T. Li, T. Zheng, J. Han, Z. Liu, Z. X. Guo, Z. Zhuang, J. Xu, B. H. Guo, *Polymers* **2019**, *11*.
[57] P. Phoungtawee, D. Crespy, *Polym. Chem.* **2021**, *12*, 3893.
[58] N. Iqbal, M. Tripathi, S. Parthasarathy, D. Kumar, P. K. Roy, *Prog. Org. Coat.* **2018**, *123*, 201.
[59] A. M. Castagna, A. Pangon, T. Choi, G. P. Dillon, J. Runt, *Macromolecules* **2012**, *45*, 8438.
[60] F. Ji, Y. Zhou, Y. Yang, *J. Mater. Chem. A* **2021**, *9*, 7172.
[61] Q. Zhou, L. Cao, Q. Li, Y. Yao, Z. Ouyang, Z. Su, X. Chen, *J. Appl. Polym. Sci.* **2012**, *125*, 3695.
[62] Y. He, X. Zhang, J. Runt, *Polymer* **2014**, *55*, 906.
[63] H. Zou, S. Wu, J. Shen, *Chem. Rev.* **2008**, *108*, 3893.
[64] S. Karimi, J. Feizy, F. Mehrjo, M. Farrokhnia, *RSC Adv.* **2016**, *6*, 23085.
[65] W. Khan, R. Sharma, P. Saini, In *Carbon Nanotubes – Current Progress of their Polymer Composites*, IntechOpen, London **2016**.
[66] G. M. Swallowe, in *Mechanical Properties and Testing of Polymers: An A–Z Reference*, (Ed.: G. M. Swallowe), Springer Netherlands, Dordrecht **1999**, pp. 281–285.
[67] T. Li, T.-Z. Zheng, Z.-X. Guo, J. Xu, B.-H. Guo, *Chin. J. Polym. Sci.* **2019**, *37*, 1257.
[68] M. Tripathi, S. Parthasarathy, D. Kumar, P. Chandel, P. Sharma, P. K. Roy, *Polym. Test.* **2020**, *86*, 106488.
[69] X. Dai, J. Xu, X. Guo, Y. Lu, D. Shen, N. Zhao, X. Luo, X. Zhang, *Macromolecules* **2004**, *37*, 5615.
[70] J. Ma, J.-H. Kim, J. Na, J. Min, G.-H. Lee, S. Jo, C. S. Kim, *ACS Omega* **2021**, *6*, 13384.
[71] M. Mohamed, H. Mohamed, M. Moustafa, A. Eid, *Egypt. J. Chem.* **2019**, *0*, 0.
[72] S. L. Tang, Y. F. Li, Y. R. Wang, Y. M. Gao, Q. L. Zheng, D. W. Yi, *Mater. Chem. Phys.* **2018**, *213*, 538.
[73] B. Pang, J. Zhang, M. Pang, P. Zhao, Z. Yang, S. Feng, J. Zhang, *Polym. Chem.* **2018**, *9*, 869.
[74] A. V. Menon, G. Madras, S. Bose, *Polym. Chem.* **2019**, *10*, 4370.
[75] J. M. Cervantes-Uc, J. I. M. Espinosa, J. V. Cauich-Rodríguez, A. Ávila-Ortega, H. Vázquez-Torres, A. Marcos-Fernández, J. San Román, *Polym. Degrad. Stab.* **2009**, *94*, 1666.
[76] M. Makaremi, P. Pasbakhsh, G. Cavallaro, G. Lazzara, Y. K. Aw, S. M. Lee, S. Milioto, *ACS Appl. Mater. Interfaces* **2017**, *9*, 17476.
[77] M. M. Calvino, L. Lisuzzo, G. Cavallaro, G. Lazzara, S. Milioto, *Thermochim. Acta* **2021**, *700*, 178940.
[78] S. Sahoo, H. Kalita, S. Mohanty, S. K. Nayak, *J. Macromol. Sci., Part A: Pure Appl. Chem.* **2017**, *54*, 819.
[79] B. Muhammad Ahsan, *Solids* **2021**, *2*, 108.
[80] D. C. H. Chin, K. Palaniandy, I. L. Hia, P. Pasbakhsh, *Polym. Compos.* **2020**, *41*, 1036.
[81] J. Zheng, R. Ozisik, R. W. Siegel, *Polymer* **2006**, *47*, 7786.
[82] T. Arunkumar, S. Ramachandran, *Int. J. Ambient Energy* **2017**, *38*, 781.
[83] K. Balani, V. Verma, A. Agarwal, R. Narayan, in *Biosurfaces: A Materials Science and Engineering Perspective*, Hoboken, NJ **2014**, pp. 329–344.
[84] S. Das, D. F. Cox, G. L. Wilkes, D. B. Klinedinst, I. Yilgor, E. Yilgor, F. L. Beyer, *J. Macromol. Sci., Part B: Phys.* **2007**, *46*, 853.
[85] R. M. Versteegen, R. Kleppinger, R. P. Sijbesma, E. W. Meijer, *Macromolecules* **2006**, *39*, 772.
[86] J. K. Park, J. Ryu, B. C. Koo, S. Lee, K. H. Kang, *Soft Matter* **2012**, *8*, 11889.
[87] L. Lisuzzo, G. Cavallaro, P. Pasbakhsh, S. Milioto, G. Lazzara, *J. Colloid Interface Sci.* **2019**, *547*, 361.
[88] E. P. Giannelis, *Appl. Organomet. Chem.* **1998**, *12*, 675.
[89] X. Pei, T. Zhang, J. Zhong, Z. Chen, C. Jiang, W. Chen, *Sci. Total Environ.* **2021**, *774*, 145705.